Discussions on the MHD adaptive solvers in the AMROC framework for space plasmas applications

M. O. Domingues, M. Moreira Lopes, R. Deiterding, O. Mendes

National Institute for Space Research (INPE), Brazil
University of Southampton, UK

ICIAM, Valencia, Spain
MS: Cartesian CFD Methods for Complex Applications
16th July, 2019

Outline

Motivation
MHD Equations
Adaptive schemes
MR refinement indicator
AMROC framework
Experiments

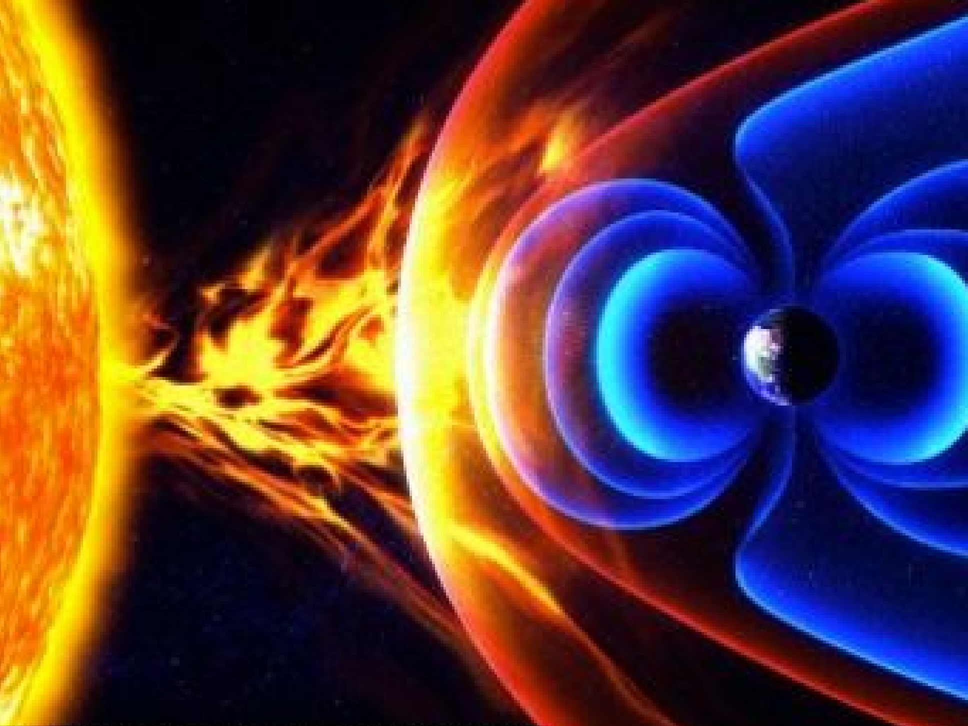

Space-physics context

Instabilities: in the magnetosphere and/or ionosphere regions

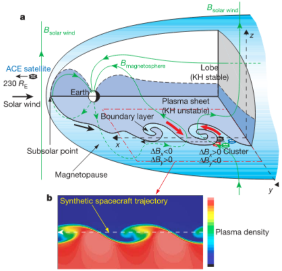

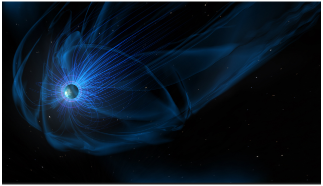

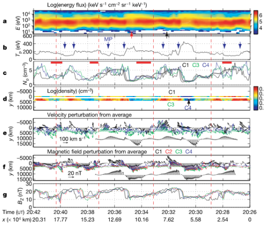

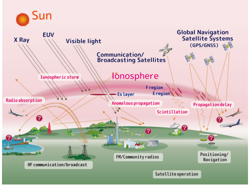

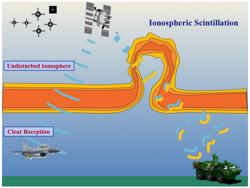

Image credits: MMS and CINDI NASA-Missions

Credits: Hasegawa et al. (2004 Nature)

http://aer.nict.go.jp/en/people/spe_yokoyama.html

Compressible Magnetohydrodynamic Equations I

$$\boxed{\frac{\partial \mathbf{q}}{\partial t} + \nabla \cdot \mathbf{f} = 0} \quad \text{with the solenoidal condition} \quad \boxed{\nabla \cdot \mathbf{B} = 0}$$

$$\boxed{\mathbf{q} = \begin{pmatrix} \rho \\ \rho\mathbf{u} \\ \mathbf{B} \\ e \end{pmatrix}} \quad \text{and} \quad \boxed{\mathbf{f} = \begin{pmatrix} \rho\,\mathbf{u} \\ \rho\mathbf{u}\mathbf{u} + \left(p + \frac{B^2}{2}\right)\mathbf{I} - \mathbf{B}\mathbf{B} \\ \mathbf{u}\mathbf{B} - \mathbf{B}\mathbf{u} \\ \left(e + p + \frac{B^2}{2}\right)\mathbf{u} - \mathbf{B}\left(\mathbf{u} \cdot \mathbf{B}\right) \end{pmatrix}}$$

$\rho = \rho(\mathbf{x}, t)$ is the density, $p = p(\mathbf{x}, t)$ is the pressure, $\mathbf{I}$ is a 3×3 identity matrix, $\mathbf{u} = \mathbf{u}(\mathbf{x}, t)$ is the velocity, $\mathbf{B} = \mathbf{B}(\mathbf{x}, t)$ is the magnetic field, $\mathbf{uu}$ or $\mathbf{BB}$ stands for a 3×3 tensor, $\mathbf{x} = (x, y, z)$, and $e = e(\mathbf{x}, t)$ is the total energy density,

$$e = \frac{p}{\gamma - 1} + \rho\frac{u^2}{2} + \frac{B^2}{2}$$

Numerical aspects

1. Approximations of MHD Equations present a numerically and computationally challenging task
2. Uniform meshes are not practical when high resolution is only needed locally.
3. Our space adaptive strategy combines finite volumes with:
   - **Wavelet based analysis: multiresolution (MR)**

     1989 Mallat after his book, Harten (1995, Comm. Pure Appl. Math.), Kaibara and Gomes (2000, Klumer/Plenum), Cohen et al (2002, Math. Comp.), Roussel et al. (2003, J. Comput. Phys.)
   - **Structured adaptive mesh refinement (SAMR)**

     [Berger and Olinger (1984, J. Comput. Phys.), Berger & Colella (1988, J. Comput. Phys.)]
4. Explicit time-space adaptation schemes are used.

Goal: Improvement of **computational efficiency** while controlling the precision using dynamically adapted meshes in space-time in an MPI parallel distributed memory patch-based AMROC framework.

This work context I

↪ We compared (serial based): **MR:** Carmen code [Roussel et al. (2003, J. Comput. Phys.)] with **SAMR:** AMROC framework [Deiterding (2011, ESAIM Proceedings), PhD Thesis, 2003] for Euler Eqs. [Deiterding (2009, ESAIM Proceedings); 2016 (Deiterding et al. SIAM JSciC)]

⋆ MR representation is more compact, while the AMROC framework is much more efficient in terms of CPU time.

↪ Then, MR alg. in the AMROC framework in its patch-based MPI parallel, exact same numerics.

⋆ We confirmed the superiority of MR compact representation in the patch-based structure. [Deiterding et al., submitted Comput.& Fluids, 2018]

↪ In meanwhile, we developed a resistive GLM-MHD MR serial solver. [Gomes et al. 2015, APNUM; PhD Thesis, 2017], then, we introduced this solver in AMROC patch based MPI parallel [Moreira Lopes et al. 2018, Comput.& Fluids, PhD Thesis, 2019].

This work context II

$\hookrightarrow$ Now, we present our results of

- $\star$ Our MHD AMROC patch-based MPI parallel solver
- $\star$ Wavelet based adaptive algorithm in this solver.

[Domingues et al. C&F 2019, Moreira Lopes, PhD Thesis 2019].

Adaptive schemes - main ideas I

$$\frac{\partial \mathbf{q}(\mathbf{x},t)}{\partial t} + \nabla \cdot \mathbf{f}\Big(\mathbf{q}(\mathbf{x},t)\Big) = \mathbf{0}$$

Numerical scheme: (2D example)

$$\mathbf{Q}_{j,k}^{n+1} = \mathbf{Q}_{j,k}^{n} - \frac{\Delta t}{\Delta x}\left[\mathbf{F}^x_{j+\frac{1}{2},k} - \mathbf{F}^x_{j-\frac{1}{2},k}\right] - \frac{\Delta t}{\Delta y}\left[\mathbf{F}^y_{j,k+\frac{1}{2}} - \mathbf{F}^y_{j,k-\frac{1}{2}}\right]$$

- **Reference scheme**: $\mathbf{Q^{n+1}} = \mathcal{D}\ \mathbf{Q^n}$

  $\mathbf{Q^n} = \mathbf{Q^{n,L}}$ cell average in a regular mesh $\mathcal{M}^L$ em $t^n = n\Delta t$

  $\mathcal{D} = \mathcal{D}^{L,\Delta t}$ stable and consistent operator in the time evolution

Adaptive schemes - main ideas II

- **Adaptive scheme**: $(\mathcal{M}^n, \mathbf{Q}_a^n) \to (\mathcal{M}^{n+1}, \mathbf{Q}_a^{n+1})$

  $\mathcal{M}^n \subset \mathcal{M}^L$ adaptive mesh Q_a^n cell average in $\mathcal{M}^n$

  Main steps:

  1. Refinement: $(\mathcal{M}^n, Q_a^n) \xrightarrow{\mathcal{R}} (\mathcal{M}^{n+}, Q_a^{n+})$
  2. Evolution: $(\mathcal{M}^{n+}, \mathbf{Q}_a^{n+}) \xrightarrow{\mathcal{D}_a} (\mathcal{M}^{n+}, \check{\mathbf{Q}}^{n+1})$
  3. Adaptation: $(\mathcal{M}^{n+}, \check{\mathbf{Q}}_a^{n+1}) \xrightarrow{\mathcal{T}_\epsilon, \eta_{\mathrm{tol}}} (\mathcal{M}^{n+1}, \mathbf{Q}_a^{n+1})$.
     - Cluster organization: if it is the case

Multiresolution (MR) MR principles of interest: I

- Two-level wavelet transform:

$$\boxed{\mathbf{Q}^{\ell+1} \rightleftharpoons \{\mathbf{Q}^{\ell}\} \cup \{\mathbf{d}^{\ell}\},}$$

- Information in a certain level can be obtained by the combination of the coarser levels with the wavelet coefficient contributions and vice-versa
- The algorithm are efficient: fast and stable.
- Wavelet coefficients $\mathbf{d}^{\ell}$ are :
  - **local approximation polynomial errors**.
  - **regularity indicators** in adaptive strategies.
  - low amplitudes of the coefficients are associated to regions where the solution is smooth
  - high amplitudes appear only in regions where the solution is less regular.

Notation:

one-dimensional example

Nested meshes:

$$\left(\Omega_k^\ell\right)_{0\leq k<2^\ell;\ 0\leq\ell\leq L}$$

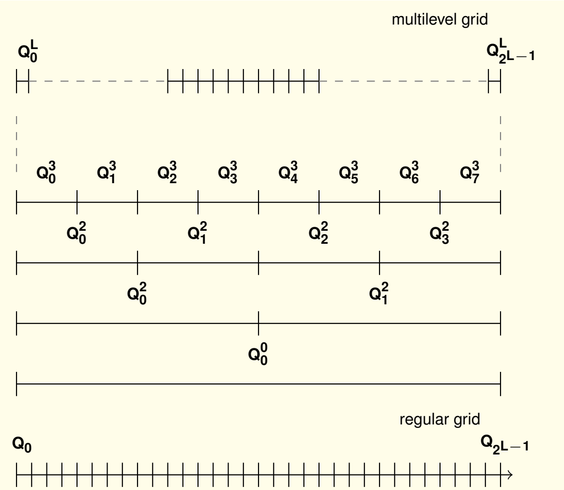

Data:

cell average value on Ω_k^ℓ :

$$Q_k^\ell = \frac{1}{|\Omega_k^\ell|}\int_{\Omega_k^\ell} Q \,\mathrm{d}\mathcal{V}$$

$\mathcal{V}$ – volume

Notation: $\mathbf{Q}^\ell = \left(\mathbf{Q}_k^\ell\right)_{0\leq k<2^\ell}$ Harten, SIAM J. Num. Anal. 1993

MR operations for FV methods

1 Projection (restriction):

$$\boxed{P_{\ell+1}^{\ell} : \mathbf{Q}^{\ell+1} \to \mathbf{Q}^{\ell}}$$

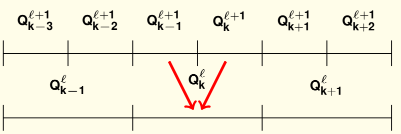

2 Prediction (prolongation):

$$\boxed{P_{\ell}^{\ell+1} : \mathbf{Q}^{\ell} \to \tilde{\mathbf{Q}}^{\ell+1}}$$

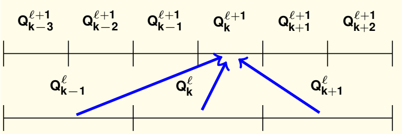

$$P_{\ell+1}^{\ell} : \mathbf{Q}_i^{\ell} = \frac{1}{2}\left(\mathbf{Q}_{2i}^{\ell+1} + \mathbf{Q}_{2i+1}^{\ell+1}\right)$$

$$P_{\ell,0}^{\ell+1} : \tilde{\mathbf{Q}}_{2i}^{\ell+1} = \mathbf{Q}_i^{\ell} - \frac{1}{8}(\mathbf{Q}_{i+1}^{\ell} - \mathbf{Q}_{i-1}^{\ell}),$$

$$P_{\ell,1}^{\ell+1} : \tilde{\mathbf{Q}}_{2i+1}^{\ell+1} = \mathbf{Q}_i^{\ell} + \frac{1}{8}(\mathbf{Q}_{i+1}^{\ell} - \mathbf{Q}_{i-1}^{\ell})$$

Linear polynomial interpolation as proposed by Harten (1995, Comm. Pure Appl. Math.).

Two-dimensional operators

Projection $P_{\ell+1}^{\ell}$:

$$\mathbf{Q}_{i,j}^{\ell} = \frac{1}{4}\left(\mathbf{Q}_{2i,2j}^{\ell+1} + \mathbf{Q}_{2i,2j+1}^{\ell+1} + \mathbf{Q}_{2i+1,2j}^{\ell+1} + \mathbf{Q}_{2i+1,2j+1}^{\ell+1}\right)$$

Prediction $P_{\ell}^{\ell+1}$ by Bihari and Harten (1995):

$$\begin{aligned}\tilde{\mathbf{Q}}_{2i+m,2j+n}^{\ell+1} &= \mathbf{Q}_{i,j}^{\ell} + \frac{1}{8}\left[(-1)^m\left(\mathbf{Q}_{i+1,j}^{\ell} - \mathbf{Q}_{i-1,j}^{\ell}\right) + (-1)^n\left(\mathbf{Q}_{i,j+1}^{\ell} - \mathbf{Q}_{i,j-1}^{\ell}\right)\right] \\ &\quad + \frac{1}{64}\left[(-1)^{mn}\left(\mathbf{Q}_{i+1,j+1}^{\ell} - \mathbf{Q}_{i+1,j-1}^{\ell} - \mathbf{Q}_{i-1,j+1}^{\ell} + \mathbf{Q}_{i-1,j-1}^{\ell}\right)\right]\end{aligned}$$

- Constructed by tensor product
- Note that these prediction operators are not TVD!

Three-dimensional operators

$$P_{\ell+1}^{\ell}: \quad \mathbf{Q}_{i,j}^{\ell} = \frac{1}{8}\Big(\mathbf{Q}_{2i,2j,2k}^{\ell+1} + \mathbf{Q}_{2i,2j+1,2k}^{\ell+1} + \mathbf{Q}_{2i+1,2j,2k}^{\ell+1} + \mathbf{Q}_{2i+1,2j+1,2k}^{\ell+1} + \mathbf{Q}_{2i,2j,2k+1}^{\ell+1} + \mathbf{Q}_{2i,2j+1,2k+1}^{\ell+1} + \mathbf{Q}_{2i+1,2j,2k+1}^{\ell+1} + \mathbf{Q}_{2i+1,2j+1,2k+1}^{\ell+1}\Big)$$

Prediction $P_{\ell}^{\ell+1}$ after Roussel et al. (2003, J. Comput. Phys.):

$$\begin{aligned}
\tilde{\mathbf{Q}}_{2i+m,2j+n,2k+p}^{\ell+1} = {} & \mathbf{Q}_{i,j,k}^{\ell} + \\
& \frac{1}{8}\Big[(-1)^{m}\left(\mathbf{Q}_{i+1,j,k}^{\ell} - \mathbf{Q}_{i-1,j,k}^{\ell}\right) + (-1)^{n}\left(\mathbf{Q}_{i,j+1,k}^{\ell} - \mathbf{Q}_{i,j-1,k}^{\ell}\right) \\
& \quad + (-1)^{p}\left(\mathbf{Q}_{i,j,k+1}^{\ell} - \mathbf{Q}_{i,j,k-1}^{\ell}\right)\Big] \\
& + \frac{1}{64}\Big[(-1)^{mn}\left(\mathbf{Q}_{i+1,j+1,k}^{\ell} - \mathbf{Q}_{i+1,j-1,k}^{\ell} - \mathbf{Q}_{i-1,j+1,k}^{\ell} + \mathbf{Q}_{i-1,j-1,k}^{\ell}\right) \\
& \qquad (-1)^{np}\left(\mathbf{Q}_{i,j+1,k+1}^{\ell} - \mathbf{Q}_{i,j-1,k+1}^{\ell} - \mathbf{Q}_{i,j+1,k-1}^{\ell} + \mathbf{Q}_{i,j-1,k-1}^{\ell}\right) \\
& \qquad (-1)^{mp}\left(\mathbf{Q}_{i+1,j,k+1}^{\ell} - \mathbf{Q}_{i-1,j,k+1}^{\ell} - \mathbf{Q}_{i+1,j,k-1}^{\ell} + \mathbf{Q}_{i-1,j,k-1}^{\ell}\right)\Big] \\
& + \frac{1}{512}\Big[\mathbf{Q}_{i+1,j+1,k+1}^{\ell} - \mathbf{Q}_{i+1,j+1,k-1}^{\ell} - \mathbf{Q}_{i+1,j-1,k+1}^{\ell} - \mathbf{Q}_{i-1,j+1,k+1}^{\ell} + \\
& \qquad \mathbf{Q}_{i+1,j-1,k-1}^{\ell} + \mathbf{Q}_{i-1,j+1,k-1}^{\ell} + \mathbf{Q}_{i-1,j-1,k+1}^{\ell} - \mathbf{Q}_{i-1,j-1,k-1}^{\ell}\Big]
\end{aligned}$$

Proprieties:

- **Localization**: finite stencil and near the cell.
- **Exact polynomial approximation.**
- **Stability**
- **Conservation**: $P_{\ell+1}^{\ell} P_{\ell}^{\ell+1}$ is the identity operator.
- Conservation implies $P_{\ell+1}^{\ell}\, \mathbf{d}^{\ell} = 0$.

Adaptive transform

- **Threshold operation:** $\rightarrow$ data compression
  modulus of the wavelet coefficients bellow certain tolerance are removed.
  MR threshold strategies: hard threshold, level dependent threshold, vector-value threshold.
- Buffer zones

Use of wavelet transform for adaptation

***Wavelet* coefficients**:

$$\boxed{\mathbf{d}^\ell = \mathbf{Q}^{\ell+\mathbf{1}} - \mathbf{P}_\ell^{\ell+\mathbf{1}}\,\mathbf{Q}^\ell \qquad \text{prediction error}}$$

Use of predicton error as refinement criterion:

$$|\mathbf{Q}^\ell - P_{\ell-1}^\ell\,P_\ell^{\ell-1}\,\mathbf{Q}^\ell| > \epsilon$$

Choice of ϵ:

Use of wavelet transform for adaptation

***Wavelet* coefficients**:

$$\boxed{\mathbf{d}^{\ell} = \mathbf{Q}^{\ell+1} - \mathbf{P}_{\ell}^{\ell+1}\,\mathbf{Q}^{\ell} \qquad \text{prediction error}}$$

Use of predicton error as refinement criterion:

$$|\mathbf{Q}^{\ell} - P_{\ell-1}^{\ell}\,P_{\ell}^{\ell-1}\,\mathbf{Q}^{\ell}| > \epsilon$$

Choice of ϵ:

- level-independent threshold parameter $\epsilon \equiv \epsilon_{\ell}$
- Harten's thresholding strategy:

$$\epsilon^{\ell} = \frac{\epsilon}{|\Omega|} 2^{2(\ell+1-L)}, \quad 0 \leq \ell < L$$

- vector-valued threshold in Eucledian norm of velocity field component of $\mathbf{Q}$

Patch-SAMR ideas in AMROC

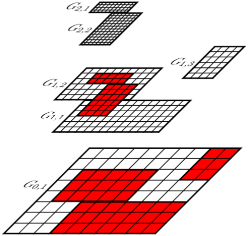

- ⋆ Block independence
- ⋆ Refined blocks overlay coarser ones

  [Berger & Colella (1988, J. Comput. Phys.)]
- ⋆ Refinement in space-time by a factor r_ℓ
- ⋆ Patch based data structures
- ⋆ Efficient cache-reuse
- ⋆ Vectorization possible

⇒ Level transfer/ setting ghost cells

- ▸ Restriction:
  Conservative averaging
- ▸ Prolongation:
  Bilinear interpolation

⇒ Linear **time interpolation** for boundary conditions

⇒ Conservative flux correction

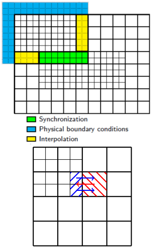

Credits: R. Deiterding, ESAIM 2011.

Patch creation by clustering

Image detection technique to identify cluster signatures.

Consider: mesh as a cluster.

Recursive cluster identification:

1. Compute # of flagged cells Υ per row/column.
2. Identify where $\Upsilon_{\text{row/col}} = 0$.
3. Compute 2^{nd} difference:

$$\boxed{\Delta = \Upsilon_{k+1} - 2\Upsilon_k + \Upsilon_{k-1}.}$$

4. Localize the largest difference in $\Delta_{\text{row/col}}$.
5. Stop $\boxed{\frac{\text{flagged cells}}{\text{unflagged cells}} < \eta_{tol}}$

$0 < \eta_{tol} < 1$

$$\eta_{tol} = \begin{cases} 0.80 & \text{parallel} \\ 0.99 & \text{equiv. serial} \end{cases}$$

[Deiterding (2011, ESAIM Proceedings); Bell et. al (1994, SIAM J. Sci. Comput.); Berger (1986, SIAM J. Sci. Stat. Comput.), and Berger & Rigoutsos (1991, IEEE Transactions on Systems)]

Numerical challenge I

The momentum equation

$$\frac{\partial \rho\,\mathbf{u}}{\partial t} + \nabla \cdot \left[\rho\,\mathbf{u}\mathbf{u} + \left(p + \frac{B^2}{2}\right)\mathbf{I} - \mathbf{B}\mathbf{B}\right] = \mathbf{0},$$

can be rewritten as

$$\frac{\partial \rho\,\mathbf{u}}{\partial t} + \nabla \cdot [\rho\,\mathbf{u}\,\mathbf{u}] + \left[\nabla\left(p + \frac{B^2}{2}\right)\right] - (\mathbf{B}\cdot\nabla)\,\mathbf{B} = \boxed{\mathbf{B}\,(\nabla\cdot\mathbf{B})}$$

- $(\nabla \cdot \mathbf{B}) = 0$ implies the non-existence of magnetic monopoles.
- $(\nabla \cdot \mathbf{B}) \neq 0$ results in a non-physical force that is parallel to $\mathbf{B}$.

$\rightarrow$ Numerically, in the **standard FV uniform scheme** $(\nabla \cdot \mathbf{B}) \neq 0$ and this exerts a destabilizing effect on the numerical scheme or possible non-physical results. [Brackbill & Barnes, 1980 J. Comput. Phys.]

Implemented solution to reduce the effects $(\nabla \cdot \mathbf{B}) \neq 0$

- We use the parabolic-hyperbolic correction to avoid this problem in conjunction with a numerical formulation of the MHD equations called Generalized Lagrangian multipliers for divergence cleaning (GLM-MHD) proposed by [Dedner et al., 2002 J. Comput. Phys.] with the dimensional adjustment proposed by [Mignone et al., 2010 J. Comput. Phys.].
- GLM introduces changes in the induction equation, a scalar function ψ and a new equation, with the parameters c_h, c_p.
- Extended-GLM (EGLM) - add also Powell's source terms. Non-conservative MHD system. [Dedner et al., 2002 J. Comput. Phys.]
- GLM (EGLM) does not zero the numerical effect but instead it transports and diffuses the numerical effect.
- Other possibility implemented is the traditional elliptic correction, it is very expensive computationally. It try to reduce this numerical effect. [Brackbill & Barnes, 1980 J. Comput. Phys.]
- $\mathcal{D}_B$ ratio between the divergence and magnitude of the magnetic field per unit of volume

Challenging test cases

⋆ Rotor (ROT)- propagation of strong torsional Alfvén waves. A high density fluid (the rotor) rotating in high velocity inside a lighter background magnetised fluid, angular momentum of the rotor to decrease and the magnetic field wraps around the rotor, increasing the magnetic pressure and compressing the fluid.

- Initial conditions:
  - → Inside rotor $\xi \leq 0.1$:
    $(\rho, u_x, u_y) = (10, -20y, -20x)$
  - → Background fluid $\xi \leq 0.1$:
    $(\rho, u_x, u_y) = (1, 0, 0)$
  - → Transition zone, elsewhere:
    $\left(9\phi + 1, -\frac{2y\phi}{\xi}, -\frac{2x\phi}{\xi}\right)$
    where $\phi = (0.115 - \xi)/0.015$,
  - → $\mathbf{B} = \left[\frac{5}{\sqrt{4\pi}}, 0, 0\right]$,
  - → The rotor is a cylinder with centre in the origin and radius 0.1
  - → ξ is distance to the origin.
- Comput. domain: $[-\frac{1}{2}, \frac{1}{2}] \times [-\frac{1}{2}, \frac{1}{2}]$,
- $T_{end} = 0.15$, $\alpha_p = 0.4$, CFL$= 0.4$, $\gamma = 1.4$
- Problem from Balsara and Spicer 1999.

⋆ Orszag-Tang (OTV) - transition to supersonic two-dimensional MHD

- Initial cond.: $\rho = \gamma^2$, $p = \gamma$,
  $\mathbf{u} = [-\sin(y), \sin(x), 0]$
  $\mathbf{B} = [-\sin(y), \sin(2x), 0]$.
- Comput. domain: $[0, 2\pi] \times [0, 2\pi]$,
- $T_{end} = \pi$, $\alpha_p = 0.5$, CFL$= 0.5$
- Problem from Orszag-Tang (1979) and others.

⋆ Spherical blast wave (BWV)- propagation of strong MHD discontinuities. Explosion of p sphere contained into a uniformly magnetised medium.

- Initial cond.: $\rho = 1$,
  $p = \begin{cases} 10, & \text{if } x^2 + y^2 < 0.1 \\ 0.1, & \text{elsewhere.} \end{cases}$,
  $\mathbf{u} = \mathbf{0}$, $\mathbf{B} = \left[\frac{\sqrt{2}}{2}, \frac{\sqrt{2}}{2}, 0\right]$,
- Comput. domain: $\left[-\frac{1}{2}, \frac{1}{2}\right] \times \left[\frac{3}{4}, \frac{3}{4}\right]$,
- $T_{end} = 0.2$, $\alpha_p = 0.5$, $CFL = 0.4$,
- Problem from Zachary et al. 1994 and others.

▶ For all cases: HLLD num. flux, MC limiter and periodic boundary conditions.

▶ For OTV and BWV: $\gamma = 5/3$.

GLM Parabolic-hyperbolic $\nabla \cdot \mathbf{B}$ correction

Moreira Lopes, PhD Thesis 2019

Uniform mesh

ROT **2D-OTV** **BWV**

$\mathcal{M}_1$

$\mathcal{M}_2$

$\mathcal{M}_3$

$\mathcal{M}_4$

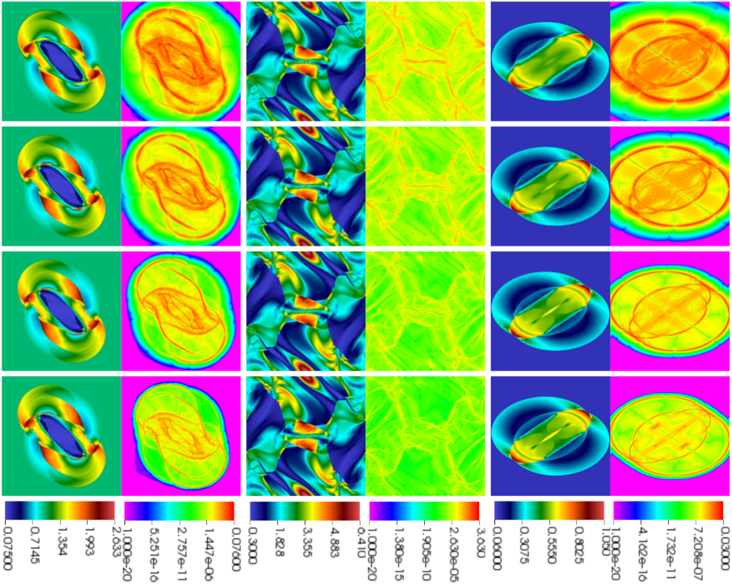

Pressure and $\mathcal{D}_B$. Parameters: $\alpha(c_p, c_h) = 0.5$, $CFL = 0.4$.

$\mathcal{M}_{1 \text{ to } 4} \rightarrow 256^2, \cdots 2048^2$ for rotor (ROT) and Orszag-Tang(OTV), $200 \times 300, \cdots 1600 \times 2400$ for blash wave (BWV) problems.

Elliptic $\nabla \cdot \mathbf{B}$ correction

Moreira Lopes, PhD Thesis 2019

Uniform mesh

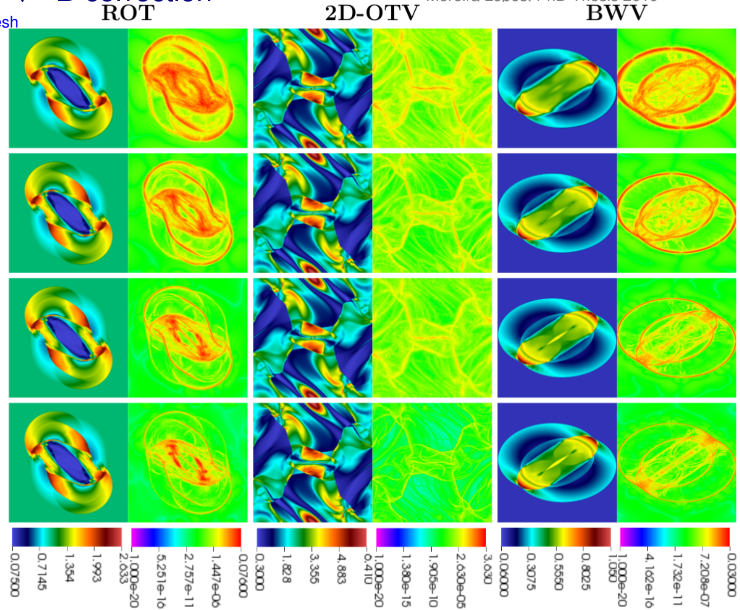

$\mathcal{M}_1$

$\mathcal{M}_2$

$\mathcal{M}_3$

$\mathcal{M}_4$

Pressure and $\mathcal{D}_B$. Parameters: $\alpha(c_p, c_h) = 0.5$, $CFL = 0.4$.

$\mathcal{M}_{1 \text{ to } 4} \rightarrow 256^2, \cdots 2048^2$ for rotor (ROT) and Orszag-Tang(OTV), $200 \times 300, \cdots 1600 \times 2400$ for blash wave (BWV) problems.

Orszag-Tang vortex

- Adaptive solution on 50×50 grid with 4 additional levels refined by $r_l = 2$
- Initial condition

$$\rho(x,y,0) = \gamma^2, \quad u_x(x,y,0) = -\sin(y), \quad u_y(x,y,0) = \sin(x), \quad u_z(x,y,0) = 0$$

$$p(x,y,0) = \gamma, \quad B_x(x,y,0) = -\sin(y), \quad B_y(x,y,0) = 2\sin(x), \quad B_z(x,y,0) = 0$$

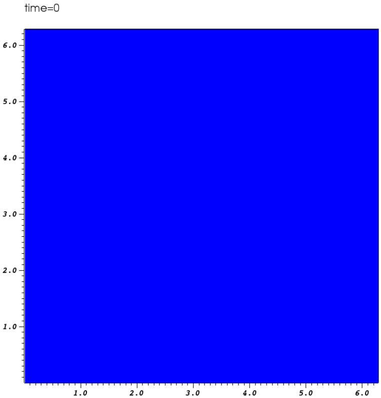

Scaled gradient of ρ

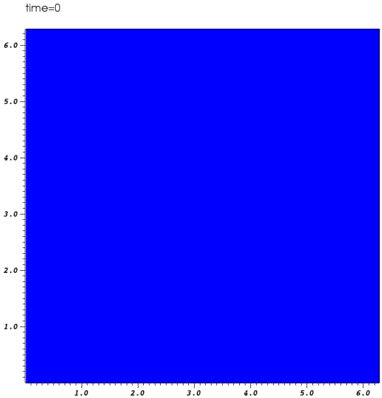

Multi-resolution criterion with hierarchical thresholding

Orszag-Tang vortex

- Adaptive solution on 50×50 grid with 4 additional levels refined by $r_l = 2$
- Initial condition

$$\rho(x,y,0) = \gamma^2, \quad u_x(x,y,0) = -\sin(y), \quad u_y(x,y,0) = \sin(x), \quad u_z(x,y,0) = 0$$

$$p(x,y,0) = \gamma, \quad B_x(x,y,0) = -\sin(y), \quad B_y(x,y,0) = 2\sin(x), \quad B_z(x,y,0) = 0$$

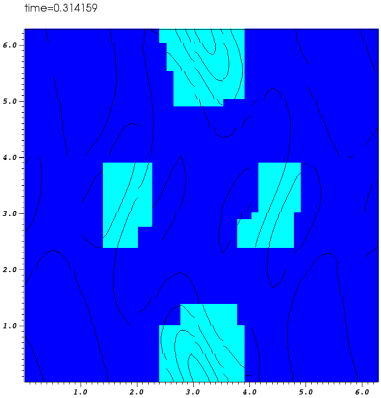

Scaled gradient of ρ

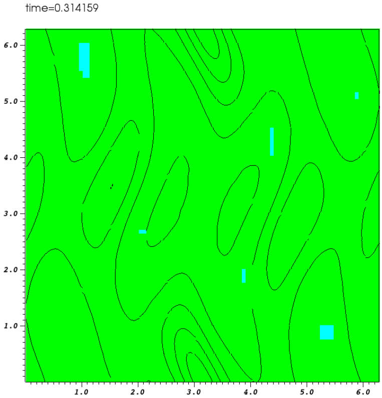

Multi-resolution criterion with hierarchical thresholding

Orszag-Tang vortex

- Adaptive solution on 50×50 grid with 4 additional levels refined by $r_l = 2$
- Initial condition

$$\rho(x,y,0) = \gamma^2, \quad u_x(x,y,0) = -\sin(y), \quad u_y(x,y,0) = \sin(x), \quad u_z(x,y,0) = 0$$

$$p(x,y,0) = \gamma, \quad B_x(x,y,0) = -\sin(y), \quad B_y(x,y,0) = 2\sin(x), \quad B_z(x,y,0) = 0$$

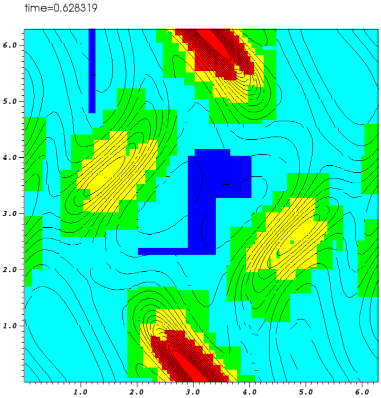

Scaled gradient of ρ

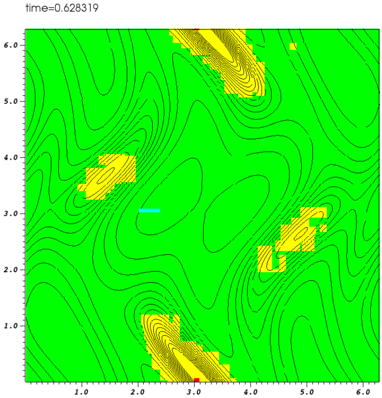

Multi-resolution criterion with hierarchical thresholding

Orszag-Tang vortex

- Adaptive solution on 50×50 grid with 4 additional levels refined by $r_l = 2$
- Initial condition

$$\rho(x,y,0) = \gamma^2, \quad u_x(x,y,0) = -\sin(y), \quad u_y(x,y,0) = \sin(x), \quad u_z(x,y,0) = 0$$

$$p(x,y,0) = \gamma, \quad B_x(x,y,0) = -\sin(y), \quad B_y(x,y,0) = 2\sin(x), \quad B_z(x,y,0) = 0$$

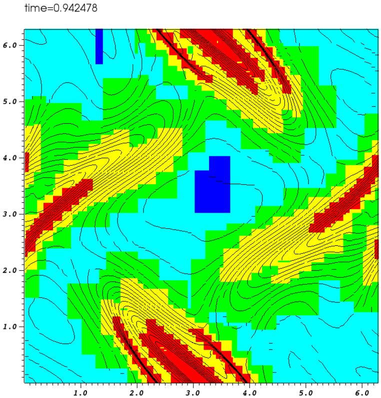

Scaled gradient of ρ

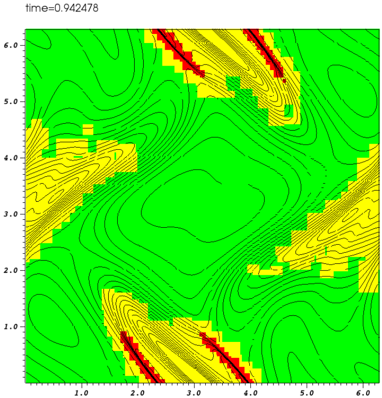

Multi-resolution criterion with hierarchical thresholding

Orszag-Tang vortex

- Adaptive solution on 50×50 grid with 4 additional levels refined by $r_l = 2$
- Initial condition

$$\rho(x,y,0) = \gamma^2, \quad u_x(x,y,0) = -\sin(y), \quad u_y(x,y,0) = \sin(x), \quad u_z(x,y,0) = 0$$

$$p(x,y,0) = \gamma, \quad B_x(x,y,0) = -\sin(y), \quad B_y(x,y,0) = 2\sin(x), \quad B_z(x,y,0) = 0$$

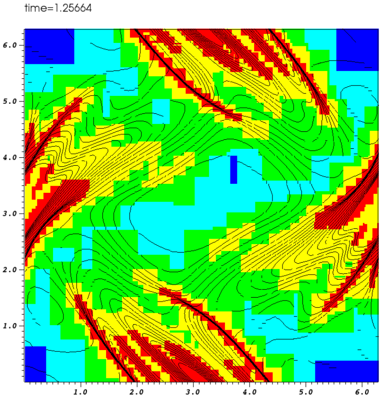

Scaled gradient of ρ

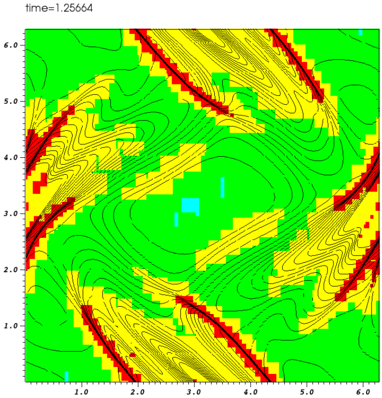

Multi-resolution criterion with hierarchical thresholding

Orszag-Tang vortex

- Adaptive solution on 50×50 grid with 4 additional levels refined by $r_l = 2$
- Initial condition

$$\rho(x,y,0) = \gamma^2, \quad u_x(x,y,0) = -\sin(y), \quad u_y(x,y,0) = \sin(x), \quad u_z(x,y,0) = 0$$

$$p(x,y,0) = \gamma, \quad B_x(x,y,0) = -\sin(y), \quad B_y(x,y,0) = 2\sin(x), \quad B_z(x,y,0) = 0$$

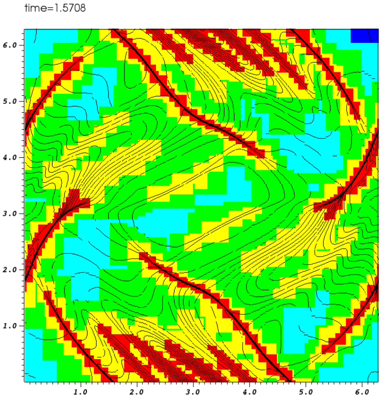

Scaled gradient of ρ

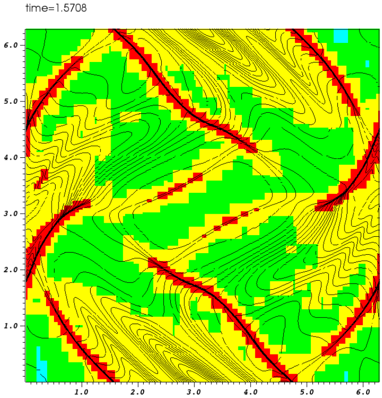

Multi-resolution criterion with hierarchical thresholding

Orszag-Tang vortex

- Adaptive solution on 50×50 grid with 4 additional levels refined by $r_l = 2$
- Initial condition

$$\rho(x,y,0) = \gamma^2, \quad u_x(x,y,0) = -\sin(y), \quad u_y(x,y,0) = \sin(x), \quad u_z(x,y,0) = 0$$

$$p(x,y,0) = \gamma, \quad B_x(x,y,0) = -\sin(y), \quad B_y(x,y,0) = 2\sin(x), \quad B_z(x,y,0) = 0$$

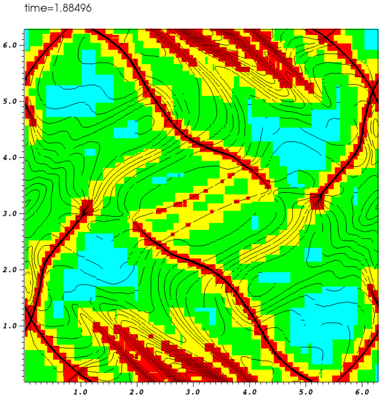

Scaled gradient of ρ

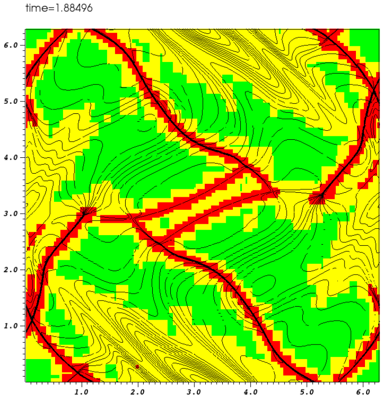

Multi-resolution criterion with hierarchical thresholding

Orszag-Tang vortex

- Adaptive solution on 50×50 grid with 4 additional levels refined by $r_l = 2$
- Initial condition

$$\rho(x,y,0) = \gamma^2, \quad u_x(x,y,0) = -\sin(y), \quad u_y(x,y,0) = \sin(x), \quad u_z(x,y,0) = 0$$

$$p(x,y,0) = \gamma, \quad B_x(x,y,0) = -\sin(y), \quad B_y(x,y,0) = 2\sin(x), \quad B_z(x,y,0) = 0$$

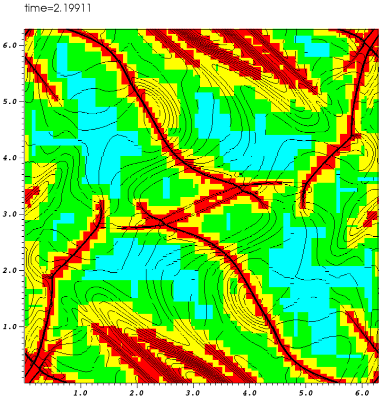

Scaled gradient of ρ

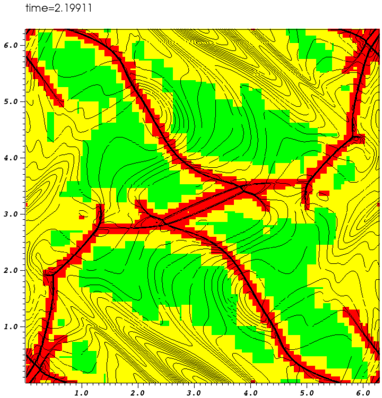

Multi-resolution criterion with hierarchical thresholding

Orszag-Tang vortex

- Adaptive solution on 50×50 grid with 4 additional levels refined by $r_l = 2$
- Initial condition

$$\rho(x,y,0) = \gamma^2, \quad u_x(x,y,0) = -\sin(y), \quad u_y(x,y,0) = \sin(x), \quad u_z(x,y,0) = 0$$

$$p(x,y,0) = \gamma, \quad B_x(x,y,0) = -\sin(y), \quad B_y(x,y,0) = 2\sin(x), \quad B_z(x,y,0) = 0$$

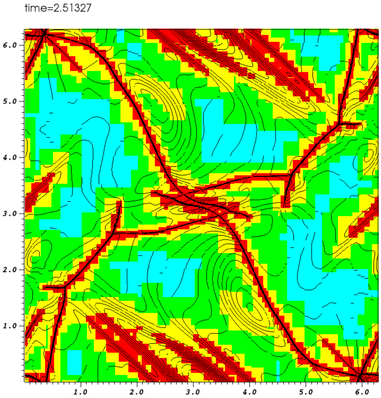

Scaled gradient of ρ

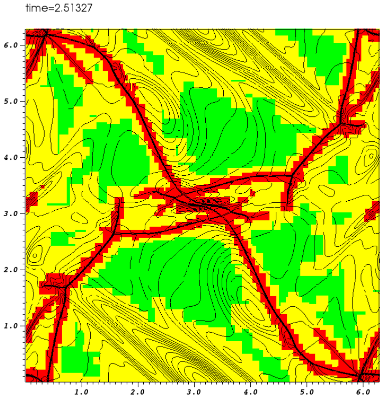

Multi-resolution criterion with hierarchical thresholding

Orszag-Tang vortex

- Adaptive solution on 50×50 grid with 4 additional levels refined by $r_l = 2$
- Initial condition

$$\rho(x,y,0) = \gamma^2, \quad u_x(x,y,0) = -\sin(y), \quad u_y(x,y,0) = \sin(x), \quad u_z(x,y,0) = 0$$

$$p(x,y,0) = \gamma, \quad B_x(x,y,0) = -\sin(y), \quad B_y(x,y,0) = 2\sin(x), \quad B_z(x,y,0) = 0$$

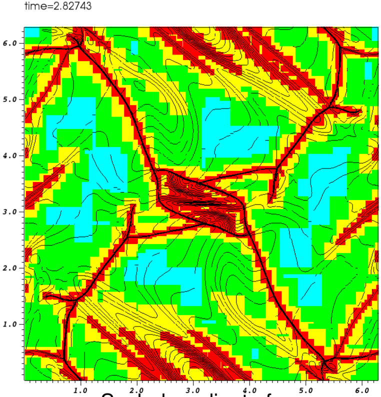

Scaled gradient of ρ

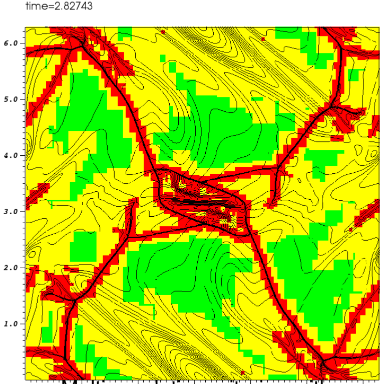

Multi-resolution criterion with hierarchical thresholding

Orszag-Tang vortex

- Adaptive solution on 50×50 grid with 4 additional levels refined by $r_l = 2$
- Initial condition

$$\rho(x,y,0) = \gamma^2, \quad u_x(x,y,0) = -\sin(y), \quad u_y(x,y,0) = \sin(x), \quad u_z(x,y,0) = 0$$

$$p(x,y,0) = \gamma, \quad B_x(x,y,0) = -\sin(y), \quad B_y(x,y,0) = 2\sin(x), \quad B_z(x,y,0) = 0$$

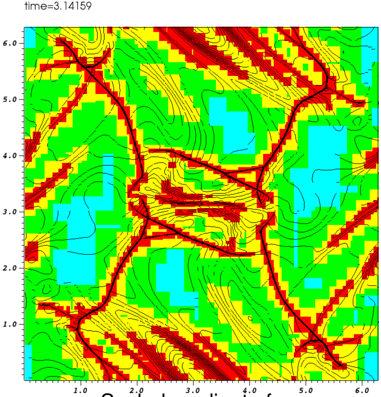

Scaled gradient of ρ

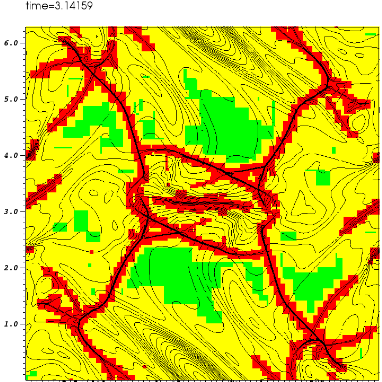

Multi-resolution criterion with hierarchical thresholding

Orszag-Tang vortex - cells on finest level vs. error

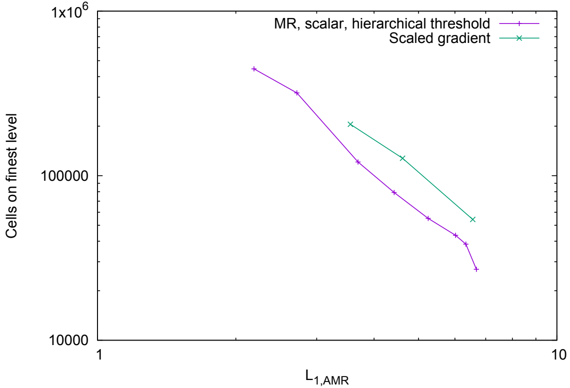

- This is work in progress, and for now, the error is evaluated in ρ only.
- Compared are SG and MR with hierarchical threshold also applied to ρ only.

Orzag-Tang vortex GLM parabolic-hyperbolic test case

Uniform Mesh

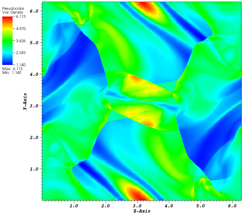

Scaled Gradient

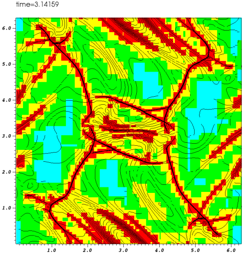

MR

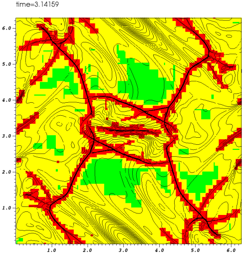

- Refinement of additional features at the maximal level with the gradient criterion and the stronger coarsening.
- These effects are the reason why the MR criterion with hierarchical thresholding achieves still a smaller error
- MR avoids unnecessary over-refinement while avoiding improper coarsening.

[Domingues et al. 2018, Comput. & Fluids]

Orzag-Tang vortex GLM parabolic-hiperbolic 3D test case

- Proposed by Helzel et al. (2011)
- a perturbation is added into the z axis of the velocity:
  $\mathbf{u} = [-[1 + 0.2\sin(z)]\sin(y), [1 + 0.2\sin(z)]\sin(x), 0.2\sin(z)]$
- Computational domain $[0, 2\pi]^3$.
- Periodic boundaries.
- Adiabatic constant $\gamma = 5/3$, $\alpha_p = 0.3$ CFL$= 0.3$ until the final time $t_{end} = \pi$.

Proc. Distribution

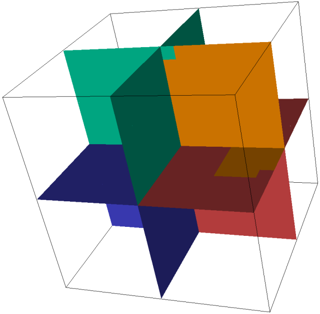

3D pressure

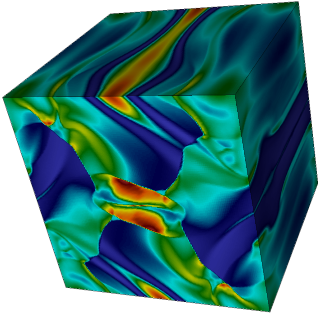

[Moreira Lopes et al. 2018, Comput. & Fluids, PhD Thesis 2019]

Kelvin-Helmholtz instability (KHI) I

The KHI is a phenomena which occur in single continuous fluids with a velocity shear.

Initial conditions (cat eye):

ρ	u_x	u_y	B_x	p
1.0	u_x^0	u_y^0	1.0	50

- Periodic boundary conditions.
- Final time = 0.4
- Computational domain of $[0, 1] \times [-1, 1]$,
- $\gamma = 1.4$, $\alpha(c_h, c_p) = 0.4$.

Adaptive solution

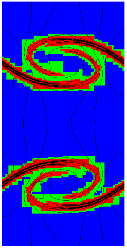

Proc. distribution

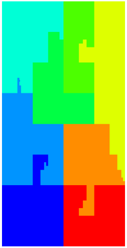

Moreira Lopes et al., 2018 Comput. & Fluids

$$u_x^0 = u_x^0(x, y) := 5 \tanh\left(20\left(y + \frac{1}{2}\right)\right) - \left[\tanh\left(20\left(y - \frac{1}{2}\right)\right) + 1\right]$$

$$u_y^0 = u_y^0(x, y) := \frac{1}{4}\sin(2\pi x)\left[e^{\left(-100\left(y+\frac{1}{2}\right)^2\right)} - e^{\left(-100\left(y-\frac{1}{2}\right)^2\right)}\right]$$

$$u_z = By = Bz = 0.$$

Dedner et al., 2002 J. Comput. Phys.

Instabilities: Rayleigh-Taylor (RTI) multi-modes

- Initial cond.(single-mode):
  - $\rho = 2$ in the upper domain and 1 in the lower domain.
  - $B_x = 0.0125$
  - Gravitational acceleration g = 0.1 must be added to the equations of motion.
  - Pressure is given by the condition of hydrostatic equilibrium, that is $p = p_0 - 0.1\rho y$, where $p_0 = 2.5$. This gives a sound speed of 3.5 in the low density medium at the interface.
  - $u_y = 0.01\ [1 + cos(4\pi x)]\ [1 + \cos(3\pi y)]\ /4$.
- Final time = 13.42
- Computational domain of $[-0.25, 0.25] \times [-0.75, 0.75]$,
- $\gamma = 1.4$, $c_h/c_p = 0.4$, ρ, 200×600, $MR_\epsilon = 0.0001$.

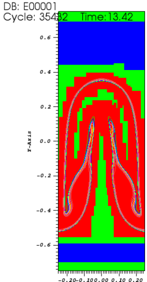

- Multi-modes
- $u_y = A\,[1 + \cos(8\pi y/3)]\ /2$, where A is a random number with a peak-to-peak amplitude of 0.01
- Pertubation zone:$[-0.1, 0.1]$
- Computational domain of

  $[-0.375, 0.375] \times [-0.75, 0.75]$.

400×1200, MR $\epsilon = 0.00005$

Test concept Jun et al., 2002 J. Comput. Phys.

- Periodic boundary cond. at $|x|$ and reflecting at $|y|$.

Final remarks

- The AMROC MHD MR–version is implemented and verified.
- Patch-based MPI-parallel distributed memory version
- Considering precision, number of cells and CPU time this new MR implementation presents better results than the scaled gradient criterion.
- We also tested more complex vector-valued wavelet criteria
- Further optimization of further SAMR core parameters stil possible
- Performance could be further increased using methods already implemented in AMROC with some more work, for instance:
  - dimensional splitting;
  - wave propagation method (fully unsplit 2nd order scheme with Roe solver);
  - higher-order WENO methods

Earth’s magnetosphere (validation, in testing)

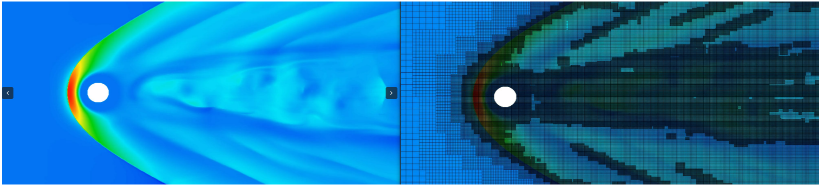

Acknowledgements

The authors thankfully acknowledge financial support from:

- CNPq - the Brazilian Research Council
- FAPESP and FAPESP SPRINT-Southampton University

Thank you !

margarete.domingues@inpe.br

Main references: I

J. Bell, M. Berger, J. Saltzman, and M. Welcome. Three-dimensional adaptive mesh refinement for hyperbolic conservation laws. SIAM J. Sci. Comput., 15(1):127–138, 1994.

M. Berger and P. Colella. Local adaptive mesh refinement for shock hydrodynamics. J. Comput. Phys., 82:64–84, 1988.

Berger, M. J., Olinger, J., 1984. Adaptive mesh refinement for hyperbolic partial differential equations. J. Comput. Phys. 53, 484–512.

M. Berger. Data structures for adaptive grid generation. SIAM J. Sci. Stat. Comput., 7(3):904{916, 1986}.

M. Berger and I. Rigoutsos. An algorithm for point clustering and grid generation. IEEE Transactions on Systems, Man, and Cybernetics, 21(5):1278{1286, 1991}.

Chiavassa, G., Donat, R., 2001. Point value multi-scale algorithms for 2D compressible flow. SIAM J. Sci. Comput. 23 (3), 805-823.

Cohen, A., Kaber, S. M., Müller, S., Postel, M., 2002. Fully adaptive multiresolution finite volume schemes for conservation laws. Math. Comp. 72, 183-225.

R. Deiterding. AMROC - Blockstructured Adaptive Mesh Refinement in Object-oriented C++. http://amroc.sourceforge.net.

R. Deiterding. Parallel adaptive simulation of multi-dimensional detonation structures. PhD thesis, Brandenburgische Technische Universität Cottbus, Sep 2003.

R. Deiterding. Construction and application of an AMR algorithm for distributed memory computers. In T. Plewa, T. Linde, and V. G. Weirs, editors, Adaptive Mesh Refinement - Theory and Applications, volume 41 of Lecture Notes in Computational Science and Engineering, pages 361–372. Springer, 2005.

R. Deiterding. A parallel adaptive method for simulating shock-induced combustion with detailed chemical kinetics in complex domains. Comp. Struct., 87:769–783, 2009.

R. Deiterding, M. O. Domingues, S. M. Gomes, O. Roussel, and K. Schneider. Adaptive multiresolution or adaptive mesh refinement? A case study for 2d Euler equations. ESAIM Proceedings, 16:181–194, 2009.

R. Deiterding. Block-structured adaptive mesh refinement - theory, implementation and application. ESAIM Proceedings, 34:97–150, 2011.

Main references: II

Deiterding, R. and Domingues, M. O. and Gomes, S. and Schneider, K. SIAM J. Sci. Comput., Comparison of adaptive multiresolution and adaptive mesh refinement applied to simulations of the compressible Euler equations., 38,5,S173-S193.

A. Harten. Multiresolution algorithms for the numerical solution of hyperbolic conservation laws. Comm. Pure Appl. Math., 48:1305–1342, 1995.

Domingues, M. O., Gomes, S. M., Roussel, O., Schneider, K., 2008. An adaptive multiresolution scheme with local time-stepping for evolutionary PDEs. J. Comput. Phys. 227(8), 3758-3780.

Gassner, G., Dumbser, M., Hindenlang, F. , Munz, C.-D., 2011. Explicit one-step time discretizations for discontinuous Galerkin and finite volume schemes based on local predictors. J. Comput. Phys. 230(11), 4232-4247.

Kaibara, M., Gomes, S. M., 2000. A fully adaptive multiresolution scheme for shock computations. In: Toro, E. F. (Ed.), Godunov Methods: Theory and Applications. Klumer/Plenum.

Hasegawa, H., Fujimoto, M., Phan, T.-D. and Rème, H., Balogh, A. Dunlop, M. W., Hashimoto, C., TanDokoro, R. *Transport of solar wind into Earth's magnetosphere through rolled-up Kelvin–Helmholtz vortices*, Nature 430, 755-758, 2004.

Bihari, B. L. and Harten, A. (1995). Application of generalized wavelets: An adaptive multiresolution scheme. *J. Comput. Appl. Math.*, 61:275–321.

Lax, P. D., Liu, X. D., 1998. Solution of two-dimensional Riemann problems of gas dynamics by positive schemes. SIAM J. Sci. Comput. 19(2), 319-340.

Müller, S., 2003. Adaptive multiscale schemes for conservation laws. Lectures Notes in Computational Science and Engineering 27, Springer, Heidelberg.

Müller, S., Stiriba, Y., 2007. Fully adaptive multiscale schemes for conservation laws employing locally varying time stepping. J. Sci. Comput. 30(3), 493-531.

Roussel, O., Schneider, K., Tsigulin, A., Bockhorn, H., 2003. A conservative fully adaptive multiresolution algorithm for parabolic PDEs. J. Comput. Phys. 188, 493-523.

Roussel, O., Schneider, 2010. Coherent Vortex Simulation of weakly compressible turbulent mixing layers using adaptive multiresolution methods. J. Comput. Phys., 229(6), 2267–2286

GLM and EGLM

GLM introduces changes in the induction equation, a scalar function ψ and a new equation, with the parameters c_h, c_p. For $2D$, we have

$$\frac{\partial B_x}{\partial t} + \frac{\partial \psi}{\partial x} + \frac{\partial}{\partial y}\left(u_y B_x - B_y u_x\right) = 0,$$

$$\frac{\partial B_y}{\partial t} + \frac{\partial}{\partial x}\left(u_x B_y - B_x u_y\right) + \frac{\partial \psi}{\partial y} = 0,$$

$$\frac{\partial B_z}{\partial t} + \frac{\partial}{\partial x}\left(u_x B_z - B_z u_x\right) + \frac{\partial}{\partial y}\left(u_y B_z - B_y u_z\right) = 0,$$

$$\frac{\partial \psi}{\partial t} + c_h^2 \left(\frac{\partial B_x}{\partial x} + \frac{\partial B_y}{\partial y}\right) = -\frac{c_h^2}{c_p^2}\psi,$$

EGLM include the source terms introduced by Powell in as a tentative to improve the correction. These terms are not conservative, then this method fail in most cases.

Orzag-Tang vortex test case details I

- The usual model problem for testing the transition to supersonic two-dimensional MHD turbulence is Orszag-Tang vortex.

Orszag and Tang, 1998 J. Fluid Mech.

- It is used to tests how robust the code is at handling the formation of MHD shocks, and shock-shock interactions and it can also provide how significant the numerical magnetic monopoles affect the numerical solutions.

Frequently, this test is also used for code comparisons.This test can present different fields values depending on the units of the MHD model used.

Since then it has been extensively compared in tests of numerical MHD simulations. A few such examples include Zachary et al. (JSC, 15, 263, 1994), Ryu et al. (ApJ, 452, 785, 1995 and ApJ, 509, 244, 1998), Dai & Woodward (ApJ, 494, 317, 1998), Jiang & Wu (JCP, 150, 561, 1999), and Londrillo & Del Zanna (ApJ, 530, 508, 2000). The problem was also studied as a model for 2-D turbulence by Dahlburg & Picone, Phys. Fluid B, 1, 2153 (1989) and Picone & Dahlburg, Phys. Fluid B, 3, 29 (1991), using Fourier spectral methods.